Pair-Density-Wave and Chiral Superconductivity in Twisted Bilayer Transition Metal Dichalcogenides

Yi-Ming Wu,[1,2,*] Zhengzhi Wu,[1,*] and Hong Yao[1,3,†]
[1]Institute for Advanced Study, Tsinghua University, Beijing 100084, China
[2]Stanford Institute for Theoretical Physics, Stanford University, Stanford, California 94305, USA
[3]State Key Laboratory of Low Dimensional Quantum Physics, Tsinghua University, Beijing 100084, China

(Received 18 October 2022; accepted 24 February 2023; published 23 March 2023)

We theoretically explore possible orders induced by weak repulsive interactions in twisted bilayer transition metal dichalcogenides (e.g., WSe_2) in the presence of an out-of-plane electric field. Using renormalization group analysis, we show that superconductivity survives even with the conventional van Hove singularities. We find that topological chiral superconducting states with Chern number $\mathcal{N} = 1, 2, 4$ (namely, $p + ip$, $d + id$, and $g + ig$) appear over a large parameter region with a moiré filling factor around $n = 1$. At some special values of applied electric field and in the presence of a weak out-of-plane Zeeman field, spin-polarized pair-density-wave (PDW) superconductivity can emerge. This spin-polarized PDW state can be probed by experiments such as spin-polarized STM measuring spin-resolved pairing gap and quasiparticle interference. Moreover, the spin-polarized PDW could lead to a spin-polarized superconducting diode effect.

DOI: 10.1103/PhysRevLett.130.126001

Introduction.—The advent of engineering moiré structures from stacking 2D materials starts an exciting path for studying intriguing electronic properties in quantum materials. Through interlayer van der Waals coupling, the spatial moiré potential profoundly modifies electronic band structures and in certain circumstances results in low-energy isolated narrow or even flat bands (moiré bands) [1–12], where interactions play a vital role in low-energy physics. From the experimental aspect, various phases have been found in magic-angle twisted bilayer graphene (TBG), including correlated insulators [13–17], superconductors [13,18–20], strange metal [21–23], magnetic phases [24–27], and quantum anomalous Hall states [28,29]. Soon after this, similar phases were also found in other forms of moiré structures including twisted double bilayer and trilayer graphene systems [30–38].

Twisted bilayer transition metal dichalcogenides (TMDs) were recently shown to be another promising and advantageous platform for simulating various correlated and topological states [39–51]. Monolayer TMD is a semiconductor with strong spin-orbit coupling [52–57]. The spin splitting in its valence band is much larger than that in the conduction band so that the topmost valence band can be used as a model for spin-polarized fermions on a Fermi surface [58]. Moreover, the finite energy gap in monolayer TMD allows for a continuous variation of the bandwidth with the twisted angle, implying a great tunability of moiré flat bands in this system compared to TBG [59]. Phases such as correlated insulators, antiferromagnetism, and stripe order have been observed in WSe_2/WS_2 heterostructure [60–64], and, in $MoTe_2/WSe_2$ moiré heterostructures, a metal-insulator transition was realized [65]. For twisted bilayer WSe_2 ($tWSe_2$), many interesting phenomena including metal-insulator transition, quantum critical behavior, and possible superconductivity (SC) were also found [66,67].

In this Letter, we explore possible orders in $tWSe_2$ with weak repulsive interactions and an electric-field-induced phase flux ϕ. Our results are presented in Fig. 1. We find

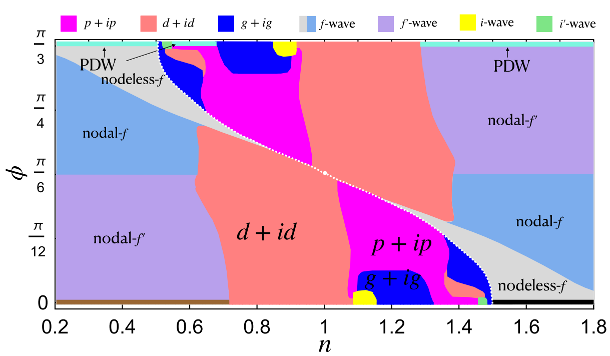

FIG. 1. Phase diagram for twisted WSe_2. At $\phi = \pi/3$, there is an emergent spin-polarized PDW with $\boldsymbol{Q} = \pm\boldsymbol{K}$ at small and large n. Centered around $n = 1$, there exist different chiral SC states which we identify as $p + ip$, $d + id$, and $g + ig$ based on their Chern numbers. At large or small n, a six-node or nodeless SC state dominates, which we denote by f or f' wave according to their representation [A_1 (B_{1u}) or A_2 (B_{2u}) of C_{3v} (D_{6h}) when $\phi > 0$ ($\phi = 0$)]. At $\phi \to 0, \pi/3$, there are tiny regimes of 12-node SC states (i and i' wave differ in their representations). The white dashed curve shows the locations of the CVHSs. $\phi = \pi/6$ and $n = 1$ is the location of the HOVHS, where the ground state is a gapless metal.

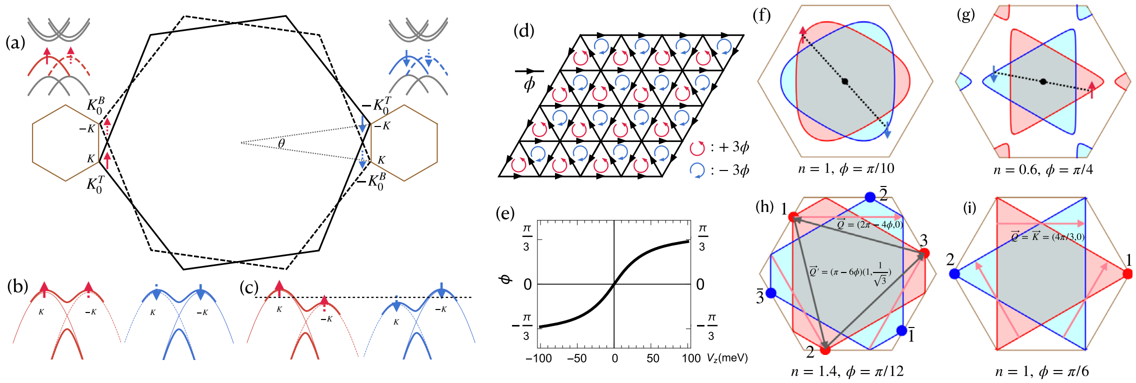

FIG. 2. (a) Formation of the moiré Brillouin zone in twisted homobilayer WSe_2. In the upper left and right insets, we show two schematic plots for both the monolayer conduction and valence band structures near $\pm K_0$. (b) Twofold degeneracy of the topmost moiré valence band, which can be lifted by an out-of-plane electric field (c). (d) The electric field effectively induces a stagger phase factor $\pm\phi$ on the bonds, leading to an accumulated flux $\pm 3\phi$ on each triangular plaquette. (e) The physical bond phase ϕ as a function of V_z, from Ref. [88]. (f)–(i) Various types of Fermi surfaces in the first Brillouin zone. Depending on the parameters, there can be electron or hole pockets, disjoint Fermi surfaces, six CVHSs, and two HOVHSs. The arrows in the last two figures are the nesting vectors. In the case of CVHS, there are two sets of nonequivalent nesting vectors $\boldsymbol{Q}$ and $\boldsymbol{Q}'$.

that there exist chiral SC states with Chern numbers $\mathcal{N} = 1, 2, 4$, corresponding to $p + ip$, $d + id$, and $g + ig$ states, respectively. For small and large filling n, the ground state is an either f- or f'-wave SC state, corresponding to A_1 or A_2 representation of the underlying C_{3v} group (or emergent D_{6h} when $\phi = 0$). The i- and i'-wave pairing states with 12 nodes belonging to different representations are also obtained. Intriguingly, at $\phi = \pi/3$ and for small or large n, the ground state features pair-density-wave (PDW) superconductivity [68–84] with equal-spin pairing. This spin-polarized PDW is degenerate with uniform SC but can become leading once a weak out-of-plane Zeeman field is applied. We argue that this PDW state can be probed by either spin-polarized STM or transport measurement of a superconducting diode effect (SDE). These SC orders survive even approaching the conventional van Hove singularities (CVHSs), shown as the white dashed curve in Fig. 1. The special point at $n = 1, \phi = \pi/6$ is the higher-order van Hove singularity (HOVHS) where the fermion density of states has a power-law divergence. We find the ground state there is a metal without symmetry breaking.

Model.—The monolayer WSe_2 is a triangular lattice semiconductor with broken inversion symmetry [52]. The valence band top is located at $\pm\boldsymbol{K}_0$, as shown in Fig. 2(a). Because of strong spin-orbit coupling, single-particle states near $\boldsymbol{K}_0$ and $-\boldsymbol{K}_0$ have opposite spin polarization. When two layers of WSe_2 are AA stacked together and twisted by a small angle, a moiré pattern and a moiré Brillouin zone develop [39,40,85–87], as shown in Fig. 2(a). The spin-up states in the top (bottom) layer near the $\boldsymbol{K}_0$ points are mapped to the states near $\boldsymbol{K}$ ($-\boldsymbol{K}$) in the moiré Brillouin zone, while the spin-down states in the top (bottom) layer near $-\boldsymbol{K}_0$ are mapped to the states near $-\boldsymbol{K}$ ($\boldsymbol{K}$). The interlayer coupling leads to a narrow moiré band, as shown in Fig. 2(b).

The presence of an emergent inversion symmetry and the time-reversal symmetry give rise to double degeneracy for each band. This degeneracy can be lifted by a finite out-of-plane electric field [see Fig. 2(c)] through the gating voltage V_z which explicitly breaks the inversion symmetry. A tight binding model for the moiré band can be obtained by constructing a set of Wannier states and fitting with density-functional theory calculations [40,66,88]. The hopping parameter t_{ij} of electrons with spin polarization σ between moiré lattice sites with $V_z \neq 0$ picks up a nontrivial phase: $t_{ij}^{\sigma} = |t_{ij}| e^{i\phi_{ij}^{\sigma}}$ and $\phi_{ij}^{-\sigma} = -\phi_{ij}^{\sigma}$ due to time-reversal symmetry. The amplitude $|t_{ij}|$ decays exponentially with distance between i and j, which allows for a nearest-neighbor (NN) hopping approximation; namely, we can set $|t_{ij}| = t$ on NN bonds and zero otherwise. The spin-dependent phase on NN bonds is $\pm\phi$, leading to an accumulated flux $\pm 3\phi$ on each triangular plaquette, as shown in Fig. 2(d). The magnitudes of ϕ depends on V_z monotonically [88], which we show in Fig. 2(e) for clarity. Moreover, it is found the on-site Coulomb repulsion is much larger than the NN interaction [66,88]. This validates the following triangular-lattice Hubbard model description:

$$H = \sum_{\boldsymbol{k},\sigma=\pm} \epsilon_{\boldsymbol{k}}^{\sigma} c_{\boldsymbol{k}\sigma}^{\dagger} c_{\boldsymbol{k}\sigma} + U \sum_{i} n_{i\uparrow} n_{i\downarrow}, \tag{1}$$

where the single-particle dispersion is given by $\epsilon_{\boldsymbol{k}}^{\sigma} = -2t \sum_{\boldsymbol{a}_m} \cos(\boldsymbol{k} \cdot \boldsymbol{a}_m + \sigma\phi)$. Hereafter, we set $\boldsymbol{a}_1 = (1, 0)$, $\boldsymbol{a}_2 = (-1/2, \sqrt{3}/2)$, and $\boldsymbol{a}_3 = (-1/2, -\sqrt{3}/2)$ in units of moiré lattice constant. For generic $\phi \neq 0$, the model respects time-reversal symmetry, spin-rotational symmetry along the z axis, and lattice symmetry C_{3v} (emergent D_{6h} for $\phi = 0$). Moreover, the model has the following symmetries regarding ϕ. First, the model is invariant by interchanging spin polarizations and changing ϕ to $-\phi$. In addition, changing the total flux on each triangular plaquette by 2π should leave the phase diagram invariant, and this corresponds to shifting ϕ by $\pm 2\pi/3$. Finally, particle-hole transformation leads to $n \to 2-n$ and $\phi \to \pi - \phi$. Consequently, the ground state phase diagram of the model is symmetric under $\phi \to \phi \pm \pi/3$ and $n \to 2-n$ [89].

Competing orders.—$\phi \neq \pi/6$, there are three nonequivalent CVHSs for each spin [Fig. 2(h)], which merge into a single HOVHS at $\phi = \pi/6$ [Fig. 2(i)]. The perfectly nested FS and divergent DOS promote the density waves (DWs) as competing orders as opposed to the SC order. To identify the leading instability in the low-energy limit, we employ the unbiased renormalization group (RG) [90–95] analysis. Since the DOS is divergent at the VHSs, it suffices to look into the small patches around them.

For the CVHS, there are six such patches, and both the bare particle-hole (ph) susceptibilities $\Pi_{ph}(\boldsymbol{Q})$ and $\Pi_{ph}(\boldsymbol{Q}')$ and the particle-particle (pp) susceptibility $\Pi_{pp}(0)$ scale as $\log^2(\Lambda/T)$, where Λ is the ultraviolet cutoff. We use $y = \Pi_{pp}(0)$ as the running parameter and define $d_1 = d\Pi_{ph}(\boldsymbol{Q})/dy$ and $d_2 = d\Pi_{ph}(\boldsymbol{Q}')/dy$ as the nesting parameters. For hexagonal lattices, the maximum value of d at perfect nesting is $1/2$ [94]. Taking the Hubbard interaction $U \approx 1t$ as the initial input, we find there is a critical value y_c where all the interactions flow to strong coupling. Near this critical point, the susceptibilities for various orders scale as $\chi \sim (y - y_c)^{\alpha}$, which signals the onset of some order only if $\alpha < 0$, and the most negative α corresponds to the leading order. In Fig. 3(a), we plot α for different competing orders as a function of $d(y_c) = d_1(y_c) \approx d_2(y_c)$. In all ranges of $d(y_c)$, the $p/d/g$-wave SC, which belongs to E representation, is the only possible order in the low T limit. Our result is consistent with the $\phi \to 0$ limit shown in Ref. [93].

For the HOVHS, there are only two patches, but all $\Pi_{pp}(0)$, $\Pi_{ph}(0)$, and $\Pi_{ph}(\boldsymbol{Q})$ scale as $1/T^{1/3}$. We again use $y = \Pi_{pp}(0)$ as the running parameter for the RG analysis and define $d_1 = \Pi_{ph}(\boldsymbol{Q})/y$ and $d_2 \approx 3\Pi_{ph}(0)/y$ as the nesting parameters ($d_1 = d_2 = 1$ for perfect nesting). The only interaction involved in this case is the intervalley density interaction. At perfect nesting, the one-loop RG equation vanishes, and, at two-loop level, the system with repulsion does not flow to strong coupling, implying no symmetry breaking [97]. In fact, there is an interacting fixed point with $d_1 = 1$, which is a non-Fermi liquid and was dubbed as supermetal in Ref. [96]. The system becomes Fermi liquid when doped away from van Hove filling but still in the gapless regime. The phase diagram is shown in Fig. 3(b). When the nesting is not perfect ($d_1 \lesssim 0.25$), DW wins over SC beyond a critical interaction, while SC is leading for weak interaction.

Away from van Hove filling, SC is the only instability in the weak coupling regime; thus, we can focus only on the SC order and employ the Raghu-Kivelson-Scalapino RG analysis [97–99] to identify the leading pairing channel, as summarized in Fig. 1. Below, we discuss two particularly interesting cases: pair-density-wave and chiral superconductivity, respectively.

Pair-density-wave.—For the particular case $\phi = \pi/3$ (more generally, $\pm\pi/3$ modulo π), both spin-up and spin-down FSs are nested in the pp channel: FSs for each spin are symmetric with respect to $\pm\boldsymbol{K}/2$ [shown as blue and red points in Figs. 4(a) and 4(b)], leading to possible spin-polarized Cooper pairs with finite $\boldsymbol{Q} = \pm\boldsymbol{K}$. Indeed, for $0 < n < 0.5$, $0.54 < n < 0.68$, and $1.29 < n < 2$, our RG results show that the ground state features degenerate same-spin pairing at $\boldsymbol{Q} = \pm\boldsymbol{K}$ and opposite-spin pairing at $\boldsymbol{Q} = 0$.

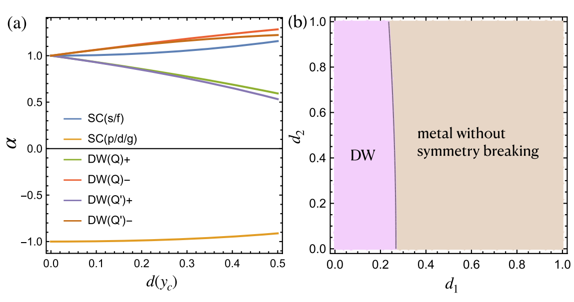

FIG. 3. (a) RG results for the CVHS near perfect nesting. The susceptibility for each order has a scaling form $\chi \sim (y - y_c)^{\alpha}$. Therefore, SC($p/d/g$) is the only possible order in the low T limit ($\pm$ in DW$\pm$ means even and odd parity). (b) Two-loop RG results of HOVHS at $\phi = \pi/6$. There is no symmetry breaking near perfect nesting, which is characterized by an interacting RG fixed point ("supermetal" in Ref. [96]). DW wins over SC at small nesting beyond a critical interaction, but SC is the only instability in weak coupling limit.

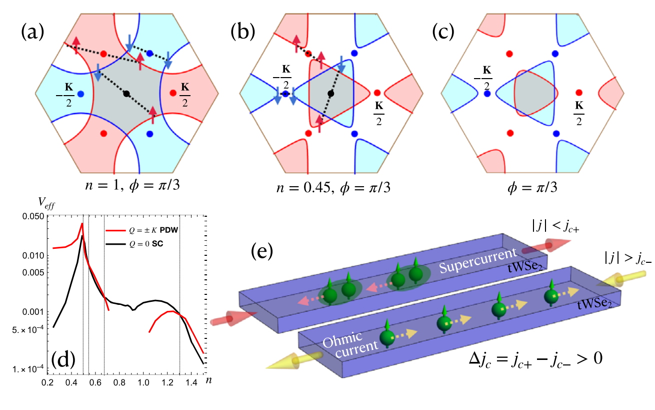

FIG. 4. (a),(b) Emergence of finite $\boldsymbol{Q}$ pairing at $\phi = \pi/3$. (c) Fermi surface with an out-of-plane Zeeman field at $\phi = \pi/3$. (d) Pairing strength of the PDW and uniform SC order. Dashed lines are their phase boundaries. (e) Experimental setup for measuring the spin-polarized SDE. An external Zeeman field is applied to favor the spin-polarized PDW. The critical currents parallel or antiparallel to $\boldsymbol{Q}$ have different magnitudes j_{c+} and j_{c-}. The applied current with magnitude between j_{c-} and j_{c+} will be Ohmic current in one direction and supercurrent in the opposite direction.

The emergence of the spin-polarized PDW order at $\phi = \pi/3$ is actually no surprise, because this particular $\phi = \pi/3$ is related to $\phi = 0$ by symmetry transformation: a particle-hole transformation plus a local gauge transformation which changes $\phi \to \phi \pm \pi/3$ and $n \to 2 - n$. Under this transformation, a triplet pairing with total $S^z = \pm 1$ at $\phi = 0$ and $2 - n$ is mapped to a PDW order at $\pi/3$ and n. Specifically, the uniform triplet pairing ($S^z = +1$) at $\phi = 0$ can be written as $\Delta_{\uparrow\uparrow}(\boldsymbol{R}, \boldsymbol{r}) c_{i\uparrow} c_{j\uparrow}$ [$\boldsymbol{R} = (\boldsymbol{r}_i + \boldsymbol{r}_j)/2$ the position of the center of mass, and $\boldsymbol{r} = \boldsymbol{r}_i - \boldsymbol{r}_j$ the relative position]. Since $\boldsymbol{Q} = 0$, $\Delta_{\uparrow\uparrow}(\boldsymbol{R}, \boldsymbol{r})$ is independent of $\boldsymbol{R}$. After the particle-hole transformation ($c_{j\sigma} \to c^\dagger_{j\sigma}$) and a local gauge transformation ($c_{j\sigma} \to e^{i\sigma\eta_j} c_{j\sigma}$ with $\eta_i = \boldsymbol{K} \cdot \boldsymbol{r}_i$), the corresponding order parameter acquires a spatial phase modulation, namely,

$$\Delta_{\uparrow\uparrow}(\boldsymbol{r}) \to \Delta_{\uparrow\uparrow}(\boldsymbol{r}) e^{i(\eta_i + \eta_j)} = \Delta_{\uparrow\uparrow}(\boldsymbol{r}) e^{i\boldsymbol{Q}\cdot\boldsymbol{R}}, \tag{2}$$

where $\boldsymbol{Q} = \boldsymbol{K} = ((4\pi/3), 0)$. For pairing between two spin-down fermions, the argument is completely parallel, but we will have $\boldsymbol{Q} = -\boldsymbol{K}$ instead. One can further see that the opposite-spin pairing ($S^z = 0$) at $\phi = 0$ is mapped to usual zero-momentum paring at $\phi = \pi/3$. This is because spin-up and spin-down sectors transform in opposite directions, $\Delta_{\uparrow\downarrow}(\boldsymbol{r}) \to \Delta_{\uparrow\downarrow}(\boldsymbol{r}) e^{i(\eta_i - \eta_j)} \sim \Delta_{\uparrow\downarrow}(\boldsymbol{r})$, which does not lead to nontrivial $\boldsymbol{R}$ dependence. Therefore, only triplet pairing state with $S^z = \pm 1$ at $\phi = 0$ transforms into a $S_z = \pm 1$ PDW order at $\phi = \pi/3$.

Since at $\phi = 0$ the $S^z = \pm 1$ triplet pairing is degenerate with the $S^z = 0$ triplet pairing due to the full spin SU(2) rotational symmetry, the system at $\phi = \pi/3$ also maintains this degeneracy between the same-spin PDW order and the opposite-spin uniform pairing. This degeneracy can be lifted by applying a weak out-of-plane magnetic field, which generates a Zeeman coupling to the spins while keeping the system in the superconducting state. Moreover, for the twisted angle $\theta \gtrsim 3°$, the orbital effect from the magnetic field can be neglected [89], leaving the Zeeman coupling the only dominant effect. In Fig. 4(c), we draw as an example the FS configurations with a finite Zeeman coupling, which differentiates the sizes of the spin-up and spin-down FSs. As a result, the $\boldsymbol{Q} = 0$ pairing between $\boldsymbol{k}$ and $-\boldsymbol{k}$ is suppressed, and the PDW becomes the unique ground state. Moreover, the degeneracy between spin-up and spin-down PDWs is also lifted by the Zeeman field: Fermions with the larger FS tend to have a stronger pairing strength and, hence, a higher T_c. To show the competition between the spin-polarized PDW and the $\boldsymbol{Q} = 0$ SC state, in Fig. 4(d) we plot the dimensionless pairing strength V_{eff} for the PDW order as well as the $\boldsymbol{Q} = 0$ SC state in a weak magnetic field. V_{eff} is defined such that $T_c \approx W \exp[-1/(V_{\mathrm{eff}} U^2/t^2)]$. For an estimation, we take $t = 5$ meV ≈ 58 K, $W = 9t$, and $U = 2.5t$; then T_c ranges from 0.18 to 9.56 K when $V_{\mathrm{eff}} \in (0.02, 0.04)$. We see that, at small n, T_c is much larger and, hence, more promising to be observed. The large n limit PDW is similar to that studied in a monolayer system [100].

This spin-polarized PDW state has the superconducting diode effect (SDE) due to the absence of inversion and time-reversal symmetry [see Fig. 4(e) for clarity], similar to that of the Fulde-Ferrell state [101]. The critical current parallel to the direction of $\boldsymbol{Q}$ is different from that in the opposite direction. As a result, an external depairing current can induce Ohmic current in one direction but remain supercurrent in the opposite direction.

Chiral superconductivity.—For the two-dimensional E representation, the gap function is $\Delta(\boldsymbol{k}) = \Delta_1 v_1(\boldsymbol{k}) + \Delta_2 v_2(\boldsymbol{k})$, where v_1 and v_2 are two *real* orthonormal basis, and the Ginzburg-Landau free energy is given by

$$\begin{aligned}\mathcal{F}[\Delta_1, \Delta_2] = {}& \alpha(T - T_c)(|\Delta_1|^2 + |\Delta_2|^2) \\ & + \beta_1(|\Delta_1|^2 + |\Delta_2|^2)^2 + \beta_2|\Delta_1^2 + \Delta_2^2|^2,\end{aligned} \tag{3}$$

where α is a positive constant and $\beta_1, \beta_2 > 0$ depends on T [97]. This free energy is minimized when $\Delta_1 = i\Delta_2$, corresponding to a chiral SC state: The phase of pairing $\varphi = \arg[\Delta(\boldsymbol{k})]$ winds up multiple times of 2π when $\boldsymbol{k}$ goes around the whole FS, while the amplitude $|\Delta(\boldsymbol{k})|$ remains nonzero on the FS (nodeless).

The nodeless chiral superconductor is topological, which supports chiral fermionic modes on edges of the system. The topological invariant is characterized by the Chern number defined as

$$\mathcal{N} = \frac{1}{4\pi} \int_{BZ} d\boldsymbol{k} [\hat{\boldsymbol{h}} \cdot (\partial_{k_x} \hat{\boldsymbol{h}} \times \partial_{k_y} \hat{\boldsymbol{h}})], \tag{4}$$

where $\hat{\boldsymbol{h}} = \{\mathrm{Re}[\Delta(\boldsymbol{k})], \mathrm{Im}[\Delta(\boldsymbol{k})], \xi_{\boldsymbol{k}}\}/E_{\boldsymbol{k}}$ and $E_{\boldsymbol{k}} = \sqrt{\xi_{\boldsymbol{k}}^2 + \Delta^2(\boldsymbol{k})}$. $2\pi\mathcal{N}$ is the Berry flux of the two-level Hamiltonian $h_k = \hat{h}(\boldsymbol{k}) \cdot \boldsymbol{\sigma}$, or the monopole charge located at the torus center, which is just the line integral of a gauge transformation on the FS, according to the Stokes theorem. In other words, Eq. (4) is the same as the winding numbers defined by the number of times that the SC phase φ slips 2π

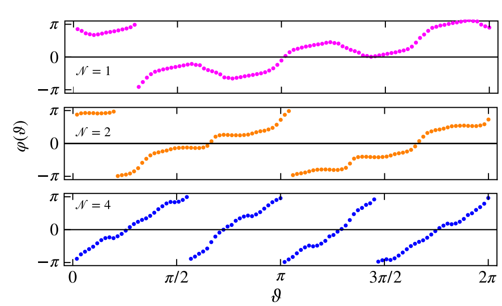

FIG. 5. SC phase variation along the FS parametrized by the angle ϑ. Distinct topological phases are characterized by the number of 2π slips when moving around the FS in a full circle.

when $\boldsymbol{k}$ sweeps around the FS [102]. There will be $2\mathcal{N}$ chiral Majorana edge modes or $\mathcal{N}$ chiral complex fermion edge modes [102–105]. In Fig. 5, we show some examples of the chiral SC states obtained in our model. We plot the SC phase φ as a function of the FS parameter ϑ. Since the FS here forms a closed loop (centered at either the $\boldsymbol{\Gamma}$ point or $\pm\boldsymbol{K}$ point), we can parametrize the points on FS by the angle ϑ formed by $\boldsymbol{k}_F$ (or $\boldsymbol{k}_F \pm \boldsymbol{K}$) and $\hat{x}$.

Concluding remarks.—We have shown that an out-of-plane electric field and magnetic field induced spin-polarized PDW order can arise in the twisted bilayer TMD system, which supports nonzero spin-polarized SC diode current, and can be directly probed using the SDE experiment [106–108]. We also find various topological chiral SC states with Chern numbers $|\mathcal{N}| = 1, 2, 4$. As disorder usually tends to suppress unconventional SC orders, sufficiently clean systems should be needed to experimentally access the exotic SC phases we obtained in the model of the twisted TMD. Various other exciting physics, such as the charge-4e superconductor or possible quantum critical behavior tuned by fields, is left for future study.

We sincerely thank Linhao Li, Zi-Xiang Li, Fengcheng Wu, and Ya-Hui Zhang for useful discussions. This work is supported in part by the MOSTC Grants No. 2021YFA1400100 and No. 2018YFA0305604 (H. Y.), the NSFC under Grant No. 11825404 (Y.-M. W., Z. W., and H. Y.), and the CAS Strategic Priority Research Program under Grant No. XDB28000000 (H. Y.). Y.-M. W. is also supported in part by Shuimu Fellow Foundation at Tsinghua and acknowledges the Gordon and Betty Moore Foundation's EPiQS Initiative through GBMF8686 for support at Stanford.

[*]These authors contributed equally to the work.
[†]yaohong@tsinghua.edu.cn

[1] J. M. B. Lopes dos Santos, N. M. R. Peres, and A. H. Castro Neto, Graphene Bilayer with a Twist: Electronic Structure, Phys. Rev. Lett. **99**, 256802 (2007).
[2] E. Suárez Morell, J. D. Correa, P. Vargas, M. Pacheco, and Z. Barticevic, Flat bands in slightly twisted bilayer graphene: Tight-binding calculations, Phys. Rev. B **82**, 121407(R) (2010).
[3] R. Bistritzer and A. H. MacDonald, Moiré bands in twisted double-layer graphene, Proc. Natl. Acad. Sci. U.S.A. **108**, 12233 (2011).
[4] G. Trambly de Laissardière, D. Mayou, and L. Magaud, Numerical studies of confined states in rotated bilayers of graphene, Phys. Rev. B **86**, 125413 (2012).
[5] P. Moon and M. Koshino, Energy spectrum and quantum Hall effect in twisted bilayer graphene, Phys. Rev. B **85**, 195458 (2012).
[6] J. M. B. Lopes dos Santos, N. M. R. Peres, and A. H. Castro Neto, Continuum model of the twisted graphene bilayer, Phys. Rev. B **86**, 155449 (2012).
[7] G. Tarnopolsky, A. J. Kruchkov, and A. Vishwanath, Origin of Magic Angles in Twisted Bilayer Graphene, Phys. Rev. Lett. **122**, 106405 (2019).
[8] H. C. Po, L. Zou, A. Vishwanath, and T. Senthil, Origin of Mott Insulating Behavior and Superconductivity in Twisted Bilayer Graphene, Phys. Rev. X **8**, 031089 (2018).
[9] L. Zou, H. C. Po, A. Vishwanath, and T. Senthil, Band structure of twisted bilayer graphene: Emergent symmetries, commensurate approximants, and wannier obstructions, Phys. Rev. B **98**, 085435 (2018).
[10] T. M. R. Wolf, J. L. Lado, G. Blatter, and O. Zilberberg, Electrically Tunable Flat Bands and Magnetism in Twisted Bilayer Graphene, Phys. Rev. Lett. **123**, 096802 (2019).
[11] M. Koshino, N. F. Q. Yuan, T. Koretsune, M. Ochi, K. Kuroki, and L. Fu, Maximally Localized Wannier Orbitals and the Extended Hubbard Model for Twisted Bilayer Graphene, Phys. Rev. X **8**, 031087 (2018).
[12] J. Kang and O. Vafek, Symmetry, Maximally Localized Wannier States, and a Low-Energy Model for Twisted Bilayer Graphene Narrow Bands, Phys. Rev. X **8**, 031088 (2018).
[13] Y. Cao, V. Fatemi, S. Fang, K. Watanabe, T. Taniguchi, E. Kaxiras, and P. Jarillo-Herrero, Unconventional superconductivity in magic-angle graphene superlattices, Nature (London) **556**, 43 (2018).
[14] Y. Xie, B. Lian, B. Jäck, X. Liu, C.-L. Chiu, K. Watanabe, T. Taniguchi, B. A. Bernevig, and A. Yazdani, Spectroscopic signatures of many-body correlations in magic-angle twisted bilayer graphene, Nature (London) **572**, 101 (2019).
[15] Y. Jiang, X. Lai, K. Watanabe, T. Taniguchi, K. Haule, J. Mao, and E. Y. Andrei, Charge order and broken rotational symmetry in magic-angle twisted bilayer graphene, Nature (London) **573**, 91 (2019).
[16] Y. Choi, J. Kemmer, Y. Peng, A. Thomson, H. Arora, R. Polski, Y. Zhang, H. Ren, J. Alicea, G. Refael, F. von Oppen, K. Watanabe, T. Taniguchi, and S. Nadj-Perge, Electronic correlations in twisted bilayer graphene near the magic angle, Nat. Phys. **15**, 1174 (2019).
[17] A. Kerelsky, L. J. McGilly, D. M. Kennes, L. Xian, M. Yankowitz, S. Chen, K. Watanabe, T. Taniguchi, J. Hone, C. Dean, A. Rubio, and A. N. Pasupathy, Maximized electron interactions at the magic angle in twisted bilayer graphene, Nature (London) **572**, 95 (2019).
[18] M. Yankowitz, S. Chen, H. Polshyn, Y. Zhang, K. Watanabe, T. Taniguchi, D. Graf, A. F. Young, and C. R. Dean, Tuning superconductivity in twisted bilayer graphene, Science **363**, 1059 (2019).
[19] X. Lu, P. Stepanov, W. Yang, M. Xie, M. A. Aamir, I. Das, C. Urgell, K. Watanabe, T. Taniguchi, G. Zhang, A. Bachtold, A. H. MacDonald, and D. K. Efetov, Superconductors, orbital magnets and correlated states in magic-angle bilayer graphene, Nature (London) **574**, 653 (2019).
[20] H. S. Arora, R. Polski, Y. Zhang, A. Thomson, Y. Choi, H. Kim, Z. Lin, I. Z. Wilson, X. Xu, J.-H. Chu, K. Watanabe, T. Taniguchi, J. Alicea, and S. Nadj-Perge, Superconductivity in metallic twisted bilayer graphene stabilized by WSe2, Nature (London) **583**, 379 (2020).
[21] H. Polshyn, M. Yankowitz, S. Chen, Y. Zhang, K. Watanabe, T. Taniguchi, C. R. Dean, and A. F. Young,

Large linear-in-temperature resistivity in twisted bilayer graphene, Nat. Phys. **15**, 1011 (2019).
[22] Y. Cao, D. Chowdhury, D. Rodan-Legrain, O. Rubies-Bigorda, K. Watanabe, T. Taniguchi, T. Senthil, and P. Jarillo-Herrero, Strange Metal in Magic-Angle Graphene with Near Planckian Dissipation, Phys. Rev. Lett. **124**, 076801 (2020).
[23] R. Lyu, Z. Tuchfeld, N. Verma, H. Tian, K. Watanabe, T. Taniguchi, C. N. Lau, M. Randeria, and M. Bockrath, Strange metal behavior of the Hall angle in twisted bilayer graphene, Phys. Rev. B **103**, 245424 (2021).
[24] A. L. Sharpe, E. J. Fox, A. W. Barnard, J. Finney, K. Watanabe, T. Taniguchi, M. A. Kastner, and D. Goldhaber-Gordon, Emergent ferromagnetism near three-quarters filling in twisted bilayer graphene, Science **365**, 605 (2019).
[25] S.-Y. Li, Y. Zhang, Y.-N. Ren, J. Liu, X. Dai, and L. He, Experimental evidence for orbital magnetic moments generated by moiré-scale current loops in twisted bilayer graphene, Phys. Rev. B **102**, 121406(R) (2020).
[26] Y. Zhang, Z. Hou, Y.-X. Zhao, Z.-H. Guo, Y.-W. Liu, S.-Y. Li, Y.-N. Ren, Q.-F. Sun, and L. He, Correlation-induced valley splitting and orbital magnetism in a strain-induced zero-energy flatband in twisted bilayer graphene near the magic angle, Phys. Rev. B **102**, 081403(R) (2020).
[27] Y. Saito, J. Ge, L. Rademaker, K. Watanabe, T. Taniguchi, D. A. Abanin, and A. F. Young, Hofstadter subband ferromagnetism and symmetry-broken Chern insulators in twisted bilayer graphene, Nat. Phys. **17**, 478 (2021).
[28] M. Serlin, C. L. Tschirhart, H. Polshyn, Y. Zhang, J. Zhu, K. Watanabe, T. Taniguchi, L. Balents, and A. F. Young, Intrinsic quantized anomalous Hall effect in a moiré heterostructure, Science **367**, 900 (2020).
[29] C.-C. Tseng, X. Ma, Z. Liu, K. Watanabe, T. Taniguchi, J.-H. Chu, and M. Yankowitz, Anomalous Hall effect at Half filling in twisted bilayer graphene, Nat. Phys. **18**, 1038 (2022).
[30] X. Liu, Z. Hao, E. Khalaf, J. Y. Lee, Y. Ronen, H. Yoo, D. Haei Najafabadi, K. Watanabe, T. Taniguchi, A. Vishwanath, and P. Kim, Tunable spin-polarized correlated states in twisted double bilayer graphene, Nature (London) **583**, 221 (2020).
[31] C. Shen, Y. Chu, Q. Wu, N. Li, S. Wang, Y. Zhao, J. Tang, J. Liu, J. Tian, K. Watanabe, T. Taniguchi, R. Yang, Z. Y. Meng, D. Shi, O. V. Yazyev, and G. Zhang, Correlated states in twisted double bilayer graphene, Nat. Phys. **16**, 520 (2020).
[32] G. Chen, L. Jiang, S. Wu, B. Lyu, H. Li, B. L. Chittari, K. Watanabe, T. Taniguchi, Z. Shi, J. Jung, Y. Zhang, and F. Wang, Evidence of a gate-tunable Mott insulator in a trilayer graphene moiré superlattice, Nat. Phys. **15**, 237 (2019).
[33] G. Chen, A. L. Sharpe, P. Gallagher, I. T. Rosen, E. J. Fox, L. Jiang, B. Lyu, H. Li, K. Watanabe, T. Taniguchi, J. Jung, Z. Shi, D. Goldhaber-Gordon, Y. Zhang, and F. Wang, Signatures of tunable superconductivity in a trilayer graphene moiré superlattice, Nature (London) **572**, 215 (2019).
[34] G. Chen, A. L. Sharpe, E. J. Fox, Y.-H. Zhang, S. Wang, L. Jiang, B. Lyu, H. Li, K. Watanabe, T. Taniguchi, Z. Shi, T. Senthil, D. Goldhaber-Gordon, Y. Zhang, and F. Wang, Tunable correlated Chern insulator and ferromagnetism in a moiré superlattice, Nature (London) **579**, 56 (2020).
[35] Y. Cao, D. Rodan-Legrain, O. Rubies-Bigorda, J. M. Park, K. Watanabe, T. Taniguchi, and P. Jarillo-Herrero, Tunable correlated states and spin-polarized phases in twisted bilayer–bilayer graphene, Nature (London) **583**, 215 (2020).
[36] M. He, Y. Li, J. Cai, Y. Liu, K. Watanabe, T. Taniguchi, X. Xu, and M. Yankowitz, Symmetry breaking in twisted double bilayer graphene, Nat. Phys. **17**, 26 (2021).
[37] J. M. Park, Y. Cao, K. Watanabe, T. Taniguchi, and P. Jarillo-Herrero, Tunable strongly coupled superconductivity in magic-angle twisted trilayer graphene, Nature (London) **590**, 249 (2021).
[38] Z. Zhu, S. Carr, D. Massatt, M. Luskin, and E. Kaxiras, Twisted Trilayer Graphene: A Precisely Tunable Platform for Correlated Electrons, Phys. Rev. Lett. **125**, 116404 (2020).
[39] F. Wu, T. Lovorn, E. Tutuc, and A. H. MacDonald, Hubbard Model Physics in Transition Metal Dichalcogenide Moiré Bands, Phys. Rev. Lett. **121**, 026402 (2018).
[40] F. Wu, T. Lovorn, E. Tutuc, I. Martin, and A. H. MacDonald, Topological Insulators in Twisted Transition Metal Dichalcogenide Homobilayers, Phys. Rev. Lett. **122**, 086402 (2019).
[41] Z. Zhang, Y. Wang, K. Watanabe, T. Taniguchi, K. Ueno, E. Tutuc, and B. J. LeRoy, Flat bands in twisted bilayer transition metal dichalcogenides, Nat. Phys. **16**, 1093 (2020).
[42] S. Shabani, D. Halbertal, W. Wu, M. Chen, S. Liu, J. Hone, W. Yao, D. N. Basov, X. Zhu, and A. N. Pasupathy, Deep moiré potentials in twisted transition metal dichalcogenide bilayers, Nat. Phys. **17**, 720 (2021).
[43] A. Weston *et al.*, Atomic reconstruction in twisted bilayers of transition metal dichalcogenides, Nat. Nanotechnol. **15**, 592 (2020).
[44] T. Devakul, V. Crépel, Y. Zhang, and L. Fu, Magic in twisted transition metal dichalcogenide bilayers, Nat. Commun. **12**, 6730 (2021).
[45] Y. Zhang, T. Liu, and L. Fu, Electronic structures, charge transfer, and charge order in twisted transition metal dichalcogenide bilayers, Phys. Rev. B **103**, 155142 (2021).
[46] M. Angeli and A. H. MacDonald, Gamma valley transition metal dichalcogenide moiré bands, Proc. Natl. Acad. Sci. U.S.A. **118**, e2021826118 (2021).
[47] K. Tran, J. Choi, and A. Singh, Moiré and beyond in transition metal dichalcogenide twisted bilayers, 2D Mater. **8**, 022002 (2020).
[48] V. Vitale, K. Atalar, A. A. Mostofi, and J. Lischner, Flat band properties of twisted transition metal dichalcogenide homo- and heterobilayers of MoS2, MoSe2, WS2 and WSe2, 2D Mater. **8**, 045010 (2021).
[49] Z. Bi and L. Fu, Excitonic density wave and spin-valley superfluid in bilayer transition metal dichalcogenide, Nat. Commun. **12**, 642 (2021).
[50] K. Slagle and L. Fu, Charge transfer excitations, pair density waves, and superconductivity in moiré materials, Phys. Rev. B **102**, 235423 (2020).

[51] L. Klebl, A. Fischer, L. Classen, M. M. Scherer, and D. M. Kennes, Competition of density waves and superconductivity in twisted tungsten diselenide, arXiv:2204.00648.

[52] S. Manzeli, D. Ovchinnikov, D. Pasquier, O. V. Yazyev, and A. Kis, 2d transition metal dichalcogenides, Nat. Rev. Mater. **2**, 17033 (2017).

[53] K. He, N. Kumar, L. Zhao, Z. Wang, K. F. Mak, H. Zhao, and J. Shan, Tightly Bound Excitons in Monolayer WSe_2, Phys. Rev. Lett. **113**, 026803 (2014).

[54] A. M. Jones, H. Yu, N. J. Ghimire, S. Wu, G. Aivazian, J. S. Ross, B. Zhao, J. Yan, D. G. Mandrus, D. Xiao, W. Yao, and X. Xu, Optical generation of excitonic valley coherence in monolayer WSe2, Nat. Nanotechnol. **8**, 634 (2013).

[55] A. Srivastava, M. Sidler, A. V. Allain, D. S. Lembke, A. Kis, and A. Imamoğlu, Valley Zeeman effect in elementary optical excitations of monolayer WSe2, Nat. Phys. **11**, 141 (2015).

[56] W. Choi, N. Choudhary, G. H. Han, J. Park, D. Akinwande, and Y. H. Lee, Recent development of two-dimensional transition metal dichalcogenides and their applications, Mater. Today **20**, 116 (2017).

[57] K. F. Mak and J. Shan, Photonics and optoelectronics of 2d semiconductor transition metal dichalcogenides, Nat. Photonics **10**, 216 (2016).

[58] D. Xiao, G.-B. Liu, W. Feng, X. Xu, and W. Yao, Coupled Spin and Valley Physics in Monolayers of MoS_2 and Other Group-VI Dichalcogenides, Phys. Rev. Lett. **108**, 196802 (2012).

[59] Z. Zhan, Y. Zhang, P. Lv, H. Zhong, G. Yu, F. Guinea, J. A. Silva-Guillén, and S. Yuan, Tunability of multiple ultraflat bands and effect of spin-orbit coupling in twisted bilayer transition metal dichalcogenides, Phys. Rev. B **102**, 241106(R) (2020).

[60] Y. Tang, L. Li, T. Li, Y. Xu, S. Liu, K. Barmak, K. Watanabe, T. Taniguchi, A. H. MacDonald, J. Shan, and K. F. Mak, Simulation of Hubbard model physics in WSe2/WS2 moiré superlattices, Nature (London) **579**, 353 (2020).

[61] E. C. Regan, D. Wang, C. Jin, M. I. Bakti Utama, B. Gao, X. Wei, S. Zhao, W. Zhao, Z. Zhang, K. Yumigeta, M. Blei, J. D. Carlström, K. Watanabe, T. Taniguchi, S. Tongay, M. Crommie, A. Zettl, and F. Wang, Mott and generalized Wigner crystal states in WSe2/WS2 moiré superlattices, Nature (London) **579**, 359 (2020).

[62] Y. Xu, S. Liu, D. A. Rhodes, K. Watanabe, T. Taniguchi, J. Hone, V. Elser, K. F. Mak, and J. Shan, Correlated insulating states at fractional fillings of moiré superlattices, Nature (London) **587**, 214 (2020).

[63] C. Jin, Z. Tao, T. Li, Y. Xu, Y. Tang, J. Zhu, S. Liu, K. Watanabe, T. Taniguchi, J. C. Hone, L. Fu, J. Shan, and K. F. Mak, Stripe phases in WSe2/WS2 moiré superlattices, Nat. Mater. **20**, 940 (2021).

[64] X. Huang, T. Wang, S. Miao, C. Wang, Z. Li, Z. Lian, T. Taniguchi, K. Watanabe, S. Okamoto, D. Xiao, S.-F. Shi, and Y.-T. Cui, Correlated insulating states at fractional fillings of the WS2/Wse2 moiré lattice, Nat. Phys. **17**, 715 (2021).

[65] T. Li, S. Jiang, L. Li, Y. Zhang, K. Kang, J. Zhu, K. Watanabe, T. Taniguchi, D. Chowdhury, L. Fu, J. Shan, and K. F. Mak, Continuous Mott transition in semiconductor moiré superlattices, Nature (London) **597**, 350 (2021).

[66] L. Wang, E.-M. Shih, A. Ghiotto, L. Xian, D. A. Rhodes, C. Tan, M. Claassen, D. M. Kennes, Y. Bai, B. Kim, K. Watanabe, T. Taniguchi, X. Zhu, J. Hone, A. Rubio, A. N. Pasupathy, and C. R. Dean, Correlated electronic phases in twisted bilayer transition metal dichalcogenides, Nat. Mater. **19**, 861 (2020).

[67] A. Ghiotto, E.-M. Shih, G. S. S. G. Pereira, D. A. Rhodes, B. Kim, J. Zang, A. J. Millis, K. Watanabe, T. Taniguchi, J. C. Hone, L. Wang, C. R. Dean, and A. N. Pasupathy, Quantum criticality in twisted transition metal dichalcogenides, Nature (London) **597**, 345 (2021).

[68] D. F. Agterberg, J. S. Davis, S. D. Edkins, E. Fradkin, D. J. Van Harlingen, S. A. Kivelson, P. A. Lee, L. Radzihovsky, J. M. Tranquada, and Y. Wang, The physics of pair-density waves: Cuprate superconductors and beyond, Annu. Rev. Condens. Matter Phys. **11**, 231 (2020).

[69] A. Larkin and Y. N. Ovchinnikov, Nonuniform state of superconductors, Sov. Phys. JETP **20**, 762 (1965).

[70] P. Fulde and R. A. Ferrell, Superconductivity in a strong spin-exchange field, Phys. Rev. **135**, A550 (1964).

[71] A. Himeda, T. Kato, and M. Ogata, Stripe States with Spatially Oscillating d-Wave Superconductivity in the Two-Dimensional $t-t'-J$ Model, Phys. Rev. Lett. **88**, 117001 (2002).

[72] E. Berg, E. Fradkin, E.-A. Kim, S. A. Kivelson, V. Oganesyan, J. M. Tranquada, and S. C. Zhang, Dynamical Layer Decoupling in a Stripe-Ordered High-T_c Superconductor, Phys. Rev. Lett. **99**, 127003 (2007).

[73] G. Y. Cho, J. H. Bardarson, Y.-M. Lu, and J. E. Moore, Superconductivity of doped Weyl semimetals: Finite-momentum pairing and electronic analog of the 3 He-A phase, Phys. Rev. B **86**, 214514 (2012).

[74] P. A. Lee, Amperean Pairing and the Pseudogap Phase of Cuprate Superconductors, Phys. Rev. X **4**, 031017 (2014).

[75] R. Soto-Garrido and E. Fradkin, Pair-density-wave superconducting states and electronic liquid-crystal phases, Phys. Rev. B **89**, 165126 (2014).

[76] S.-K. Jian, Y.-F. Jiang, and H. Yao, Emergent Spacetime Supersymmetry in 3d Weyl Semimetals and 2d Dirac Semimetals, Phys. Rev. Lett. **114**, 237001 (2015).

[77] M. Raczkowski, M. Capello, D. Poilblanc, R. Frésard, and A. M. Oleś, Unidirectional d-wave superconducting domains in the two-dimensional $t-j$ model, Phys. Rev. B **76**, 140505(R) (2007).

[78] F. Loder, S. Graser, A. P. Kampf, and T. Kopp, Mean-Field Pairing Theory for the Charge-Stripe Phase of High-Temperature Cuprate Superconductors, Phys. Rev. Lett. **107**, 187001 (2011).

[79] X. Y. Xu, K. T. Law, and P. A. Lee, Pair Density Wave in the Doped $t-j$ Model with Ring Exchange on a Triangular Lattice, Phys. Rev. Lett. **122**, 167001 (2019).

[80] J. Venderley and E.-A. Kim, Evidence of pair-density wave in spin-valley locked systems, Sci. Adv. **5**, eaat4698 (2019).

[81] J. F. Dodaro, H.-C. Jiang, and S. A. Kivelson, Intertwined order in a frustrated four-leg $t-j$ cylinder, Phys. Rev. B **95**, 155116 (2017).

[82] P. Corboz, T. M. Rice, and M. Troyer, Competing States in the t-j Model: Uniform d-Wave State Versus Stripe State, Phys. Rev. Lett. **113**, 046402 (2014).

[83] Z. Han, S. A. Kivelson, and H. Yao, Strong Coupling Limit of the Holstein-Hubbard Model, Phys. Rev. Lett. **125**, 167001 (2020).

[84] K. S. Huang, Z. Han, S. A. Kivelson, and H. Yao, Pair-density-wave in the strong coupling limit of the Holstein-Hubbard model, npj Quantum Mater. **7**, 17 (2022).

[85] M. H. Naik and M. Jain, Ultraflatbands and Shear Solitons in Moiré Patterns of Twisted Bilayer Transition Metal Dichalcogenides, Phys. Rev. Lett. **121**, 266401 (2018).

[86] D. A. Ruiz-Tijerina and V. I. Fal'ko, Interlayer hybridization and moiré superlattice minibands for electrons and excitons in heterobilayers of transition-metal dichalcogenides, Phys. Rev. B **99**, 125424 (2019).

[87] M. H. Naik, S. Kundu, I. Maity, and M. Jain, Origin and evolution of ultraflat bands in twisted bilayer transition metal dichalcogenides: Realization of triangular quantum dots, Phys. Rev. B **102**, 075413 (2020).

[88] H. Pan, F. Wu, and S. Das Sarma, Band topology, Hubbard model, Heisenberg model, and Dzyaloshinskii-Moriya interaction in twisted bilayer wse_2, Phys. Rev. Res. **2**, 033087 (2020).

[89] J. Zang, J. Wang, J. Cano, and A. J. Millis, Hartree-Fock study of the moiré Hubbard model for twisted bilayer transition metal dichalcogenides, Phys. Rev. B **104**, 075150 (2021).

[90] A. T. Zheleznyak, V. M. Yakovenko, and I. E. Dzyaloshinskii, Parquet solution for a flat fermi surface, Phys. Rev. B **55**, 3200 (1997).

[91] N. Furukawa, T. M. Rice, and M. Salmhofer, Truncation of a Two-Dimensional Fermi Surface due to Quasiparticle Gap Formation at the Saddle Points, Phys. Rev. Lett. **81**, 3195 (1998).

[92] A. V. Chubukov, D. V. Efremov, and I. Eremin, Magnetism, superconductivity, and pairing symmetry in iron-based superconductors, Phys. Rev. B **78**, 134512 (2008).

[93] R. Nandkishore, L. S. Levitov, and A. V. Chubukov, Chiral superconductivity from repulsive interactions in doped graphene, Nat. Phys. **8**, 158 (2012).

[94] Y.-P. Lin and R. M. Nandkishore, Chiral twist on the high-T_c phase diagram in moiré heterostructures, Phys. Rev. B **100**, 085136 (2019).

[95] Y.-T. Hsu, F. Wu, and S. Das Sarma, Spin-valley locked instabilities in moiré transition metal dichalcogenides with conventional and higher-order Van Hove singularities, Phys. Rev. B **104**, 195134 (2021).

[96] H. Isobe and L. Fu, Supermetal, Phys. Rev. Res. **1**, 033206 (2019).

[97] See Supplemental Material at http://link.aps.org/supplemental/10.1103/PhysRevLett.130.126001 for the symmetry classification of the pairing gap function, the details of the renormalization group analysis and the Ginzburg-Landau free energy analysis.

[98] S. Raghu, S. A. Kivelson, and D. J. Scalapino, Superconductivity in the repulsive Hubbard model: An asymptotically exact weak-coupling solution, Phys. Rev. B **81**, 224505 (2010).

[99] W. Cho, R. Thomale, S. Raghu, and S. A. Kivelson, Band structure effects on the superconductivity in Hubbard models, Phys. Rev. B **88**, 064505 (2013).

[100] Y.-T. Hsu, A. Vaezi, M. H. Fischer, and E.-A. Kim, Topological superconductivity in monolayer transition metal dichalcogenides, Nat. Commun. **8**, 14985 (2017).

[101] A. Daido, Y. Ikeda, and Y. Yanase, Intrinsic Superconducting Diode Effect, Phys. Rev. Lett. **128**, 037001 (2022).

[102] A. M. Black-Schaffer and C. Honerkamp, Chirald-wave superconductivity in doped graphene, J. Phys. Condens. Matter **26**, 423201 (2014).

[103] M. Sato and Y. Ando, Topological superconductors: A review, Rep. Prog. Phys. **80**, 076501 (2017).

[104] N. Read and D. Green, Paired states of fermions in two dimensions with breaking of parity and time-reversal symmetries and the fractional quantum Hall effect, Phys. Rev. B **61**, 10267 (2000).

[105] A. M. Black-Schaffer, Edge Properties and Majorana Fermions in the Proposed Chiral d-Wave Superconducting State of Doped Graphene, Phys. Rev. Lett. **109**, 197001 (2012).

[106] F. Ando, Y. Miyasaka, T. Li, J. Ishizuka, T. Arakawa, Y. Shiota, T. Moriyama, Y. Yanase, and T. Ono, Observation of superconducting diode effect, Nature (London) **584**, 373 (2020).

[107] Y.-Y. Lyu, J. Jiang, Y.-L. Wang, Z.-L. Xiao, S. Dong, Q.-H. Chen, M. V. Milošević, H. Wang, R. Divan, J. E. Pearson, P. Wu, F. M. Peeters, and W.-K. Kwok, Superconducting diode effect via conformal-mapped nanoholes, Nat. Commun. **12**, 2703 (2021).

[108] C. Baumgartner, L. Fuchs, A. Costa, S. Reinhardt, S. Gronin, G. C. Gardner, T. Lindemann, M. J. Manfra, P. E. Faria Junior, D. Kochan, J. Fabian, N. Paradiso, and C. Strunk, Supercurrent rectification and magnetochiral effects in symmetric Josephson junctions, Nat. Nanotechnol. **17**, 39 (2022).